International Journal of Earth Sciences (2019) 108:1493–1507
https://doi.org/10.1007/s00531-019-01716-8

ORIGINAL PAPER

Lateral variation of aeromagnetic anomaly in South China and its tectonic implications

Xiaosan Zhu[1] · Hongwei Zheng[1] · Minjie Lu[1]

Received: 25 June 2018 / Accepted: 5 April 2019 / Published online: 12 April 2019

Abstract
We present a series of images from the aeromagnetic data observed in South China areas, and reveal the detailed structures of the South China Block. By using lateral variation of the aeromagnetic anomalies, we characterize individual geological blocks and suggest the deep boundaries of the blocks. The Yangtze Block and Jiangnan orogenic belt are characterized by low aeromagnetic anomalies, whereas high values of the aeromagnetic anomaly are observed in the Cathaysia Block. The boundary between the Yangtze and Cathaysia blocks, which remains unclear to date, can be plotted along the large magnetic gradients. The high magnetic anomalies significantly relate to volcanic distributions in South China areas. These aeromagnetic observations seem to be useful to investigate the intracontinental tectonic evolution in this region.

Keywords Aeromagnetic data · Derivative enhancement · Tectonic boundary · South China

Introduction

The South China Block (SCB), a major continental block of East Asia, situates to the south of the Qinling–Dabie orogen and east of the Qinghai–Tibet plateau. It consists mainly of the Yangtze Block in the northwest and the Cathaysia Block in the southeast (Charvet et al. 1996; Wang et al. 2010a; Zhang et al. 2013; Charvet 2013; Li et al. 2014; Faure et al. 2016), and the Jiangshan–Shaoxing Fault represents the eastern part of a Neoproterozoic ophiolitic suture between the two blocks (Wang et al. 2003; Shu 2012; Chu et al. 2012a). The major part of the continent was formerly the Paleo-South China plate, which formed during the Neoproterozoic (Charvet et al. 1996, 2010; Chu et al. 2012a, b, c; Charvet 2013; Faure et al. 2016). Characteristics of the Neoproterozoic geology indicate that the SCB has experienced long-term, multi-phased tectonic changes, including intracontinental tectonism (Zhang et al. 2013). In the present day, the SCB basically consists of the metamorphic and crystalline basement and the three Phanerozoic strata, including metamorphic marine sedimentary strata, marine sedimentary strata and continental sedimentary strata from bottom to top (Chen et al. 1991, 1998; Charvet et al. 1996; Xiong et al. 2002; Shu 2012; Zhang et al. 2013).

The crystalline basement of the SCB formed during the period from the Archaeozoic to Paleoproterozoic (Shu 2012; Chu et al. 2012a, b, c). Since the Meso- to Neoproterozoic eras, the SCB has been involved in tectonism related to the assembly and breakup of the global supercontinent Rodinia and the subsequent transition of the separation and collision between the north and south continental blocks (Guo et al. 1963; Wang and Li 2003; Wang et al. 2010a; Shu 2012; Zhang et al. 2013; Hu et al. 2015).

Since the Meso-Cenozoic, the SCB has been located at the collision zone of three plates and has been a key component in the tectonic evolution toward the modern plate configuration; that is, the westerly subduction of the west Pacific plate, the formation of the Tibetan plateau and the effect of the uncoordinated movement between the Indian and Australian plates. The SCB has consequently evolved into an isolated continent, for which its movements are limited by those of its adjacent plates (Shu 2012; He et al. 2013; Deng et al. 2014; Zhao et al. 2013; Zhang et al. 2013). Since the 1970s, the tectonic structure of the SCB has been explained in the perspective of plate tectonics and a hypothesis is proposed that the SCB has experienced these evolutions of trench, island arc and basin structures stages (Guo et al. 1996; Shu 2012; Chu et al. 2012a, b, c; Charvet 2013).

✉ Xiaosan Zhu
zhuxiaosan@yahoo.com

[1] Institute of Geology, Chinese Academy of Geological Sciences, No. 26 Baiwanzhuang Road, Xicheng District, Beijing 100037, People's Republic of China

The Jiangnan orogen, hundreds of kilometers in width, is situated in the western part of the junction zone between the Yangtze and Cathaysia blocks. The Jiangnan orogen formed by the amalgamation of the Yangtze and Cathaysia blocks over a protracted period of time (Charvet 2013). The Jiangnan orogen has the largest exposed area of a Proterozoic tectonic–magmatic belt in China and is an ideal place for studying the tectonic evolution of the Yangtze and Cathaysia blocks (Qiu et al. 1998; Shu 2012). The Qinling–Dabie orogenic belt is located on the northern side of the mountain belt, and the Sichuan Basin is situated on the western side (Ding et al. 2007; Tang et al. 2011; Li et al. 2011).

It has long been considered that the SCB formed by the collision and juxtaposition of the Yangtze and Cathaysia blocks (Guo et al. 1996; Yuan and Hua, 2011; Shu 2012; Zhang et al. 2013; Hu et al. 2015). Although it has been reworked by intracontinental tectonic processes in the Mesozoic (Wang et al. 2003; Li et al. 2007; He et al. 2013), the orogenic belt should record fundamental geodynamic information of the SCB. During the Rodinia supercontinent assembly and via the early and middle Neoproterozoic amalgamation, if the separated terranes of the Mesoproterozoic SCB formed the middle Neoproterozoic ancient South China plate (Zhang et al. 2013), where is the collision boundary of the Yangtze and Cathaysia blocks and what are the physical scopes of the two blocks in the middle Neoproterozoic? In the early Paleozoic, did the granitic magmatism in South China plate result from the interaction between the Yangtze and Cathaysia blocks (He et al. 2013; Zhang et al. 2013) or originated from subduction and collision (Chen et al. 1995; Li and Li 2007; Yuan and Hua 2011)? Is there some geophysical evidence for solving this question?

The aeromagnetic data are very convenient, useful and effective where bedrocks are covered by soil, sand and water or forest. Magnetic anomaly data reveal the variations in spatial distributions and types of magnetic minerals in the crust of the earth, ignoring the effects of nonmagnetic cover and rocks. Magnetic anomaly data can also visualize the geological structural characteristics such as faults and folds. In this paper, we reveal the detailed boundary structures of the Yangtze and Cathaysia blocks and their structural characteristics in middle Neoproterozoic, and provide the geophysical evidences of interaction between the Yangtze and Cathaysia blocks during the Paleozoic based on processing and interpretation of aeromagnetic data in SCB. The study provides important new geological information of the SCB (Fig. 1).

The outline of this paper is the following. Firstly, we briefly introduce the geological settings of SCB, and we present the rocks and magnetic field in South China. We then provide the collection information of aeromagnetic data in South China and describe five processing methods of data. Following that, we interpret the lateral variation of the aeromagnetic anomalies in South China and discuss its tectonic implications. Finally, we give some conclusions.

Geological settings

The SCB (Fig. 1) has an Archaeozoic–Paleoproterozoic crystalline basement, widely distributed early continental crust residual materials and Archean materials according to the previous studies (Liu et al. 2006; Shu 2006, 2012; Wang et al. 2007; Zhang et al. 2013), such as the Archaeozoic (~3.3–2.9 Ga) Kongling complex in the Yangtze Block (Zhang et al. 2006, 2013), the Paleoproterozoic (~2.5–1.9 Ga) Badu group (Yu et al. 2010; Peng et al. 2012) and the Mesoproterozoic (~1.68 Ga) Dahongshan group (Li et al. 2007; Zhang et al. 2013). The tectonic evolution of the SCB involved the collision and the subsequent rifting of the global supercontinent Rodinia (Li et al. 2007; Zhang et al. 2013).

The Yangtze and Cathaysia blocks have distinct Precambrian basement as a result of different evolutionary histories during the Archean to Neoproterozoic period (Charvet 2013; Li et al. 2014; Shu et al. 2015). The basement of the Yangtze Block is composed of high-grade metamorphosed tonalite, trondhjemite, granodiorite gneisses and amphibolites (Zheng and Zhang 2007; Li et al. 2014). These rocks have experienced intense deformation and amphibolite facies metamorphism, which resulted from the assembly of the supercontinent Columbia during the Paleoproterozoic period (Zheng and Zhang 2007; Li et al. 2014). In the Yangtze Block, there are some differences in the lithospheric characteristics between the eastern and central parts of the block. The eastern part is dominated by the lower Paleozoic strata composed mainly of carbonate rocks and siliciclastic materials. The Cambrian strata are mainly composed of slate and limestone, Ordovician strata are mainly limestone with some siltstone and sandstone, and Lower Silurian strata are dominantly sandstone and shale (Wang et al. 2010a). For the western part, the Cambrian strata are mainly composed of carbonate, the Ordovician strata are composed of limestone, shale and muddy sandstone, and the Lower and Middle Silurian strata are composed of thick shale and sandstone (Wang et al. 2010a).

Compared with the Yangtze Block, the basement of the Cathaysia Block is composed of Paleoproterozoic to Neoproterozoic schist, gneiss, amphibolite, migmatite and metavolcanic rocks (Wang et al. 2010a; Li et al. 2014). Most of the basement rocks are unconformably overlain by Neoproterozoic to Ordovician rocks (Wang et al. 2010a; Li et al. 2014). The Cambrian strata in the Cathaysia Block are composed of sandstone, siltstone, mudstone and limestone, which are different from the lithological characteristics of rocks on the west side of the Chenzhou–Linwu fault (Wang et al. 2010a). The Lower to Middle Ordovician strata are composed of phyllite, slate, sandstone, mudstone and limestone (Wang et al. 2010a).

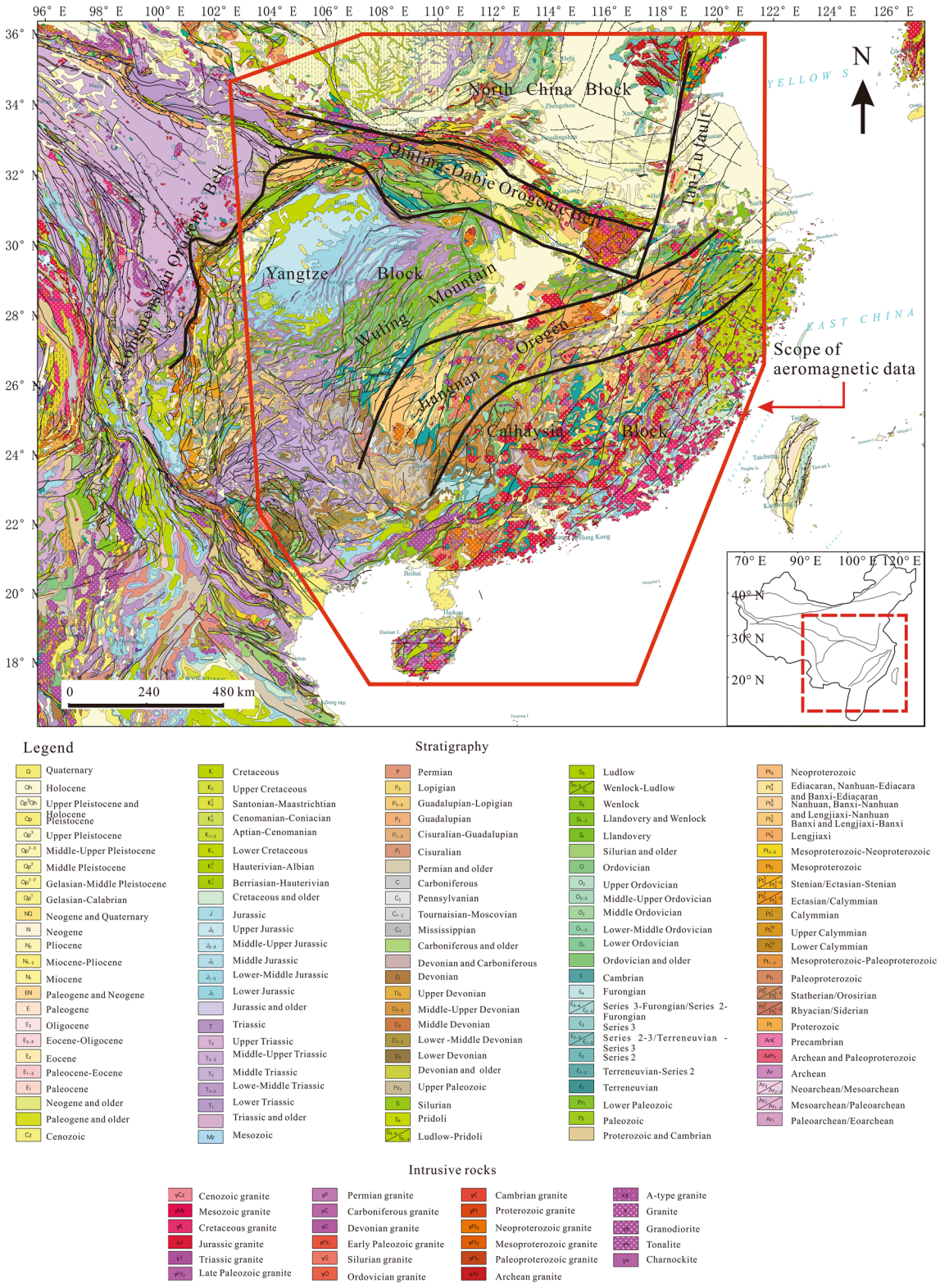

Fig. 1 Geological map showing the study areas (red polygon) of South China (after Shu 2012; Charvet 2013; Ren 2015)

Rocks and magnetic field in south china

The magnetic fields are intrinsic characteristics of rocks, ore bodies and geological structures. The magnetic susceptibilities of rocks are closely related to their chemical compositions and structures. The magnetic properties of rocks are generally related to the contents of ferromagnetic materials and the magnetic susceptibilities of rocks of a same kind of lithology are enhanced with the increasing mafic mineral contents. In general, rocks formed from crustal sources have weak magnetic susceptibilities, those formed from mixed crustal and mantle sources have intermediate magnetic susceptibilities and those formed from the mantle materials have strong magnetic susceptibilities. Magnetic susceptibility anomalies are comprehensive results of the magnetic materials, both in the shallow and deep parts of the lithosphere.

Several general observations can be made from the magnetic susceptibility statistics of the rocks in the SCB (Table 1). Basic to neutral volcanic rocks, though variable, generally have high magnetic susceptibilities. Basalt and andesite basalt have high magnetic susceptibilities, whereas the magnetic susceptibilities of andesitic breccia and andesite have intermediate values, and the magnetic susceptibilities of trachyte and tuff are small (Table 1). The magnetic susceptibilities of intrusive rocks increase from the magnetic susceptibilities of acid rocks to those of basic ones. The magnetic susceptibilities of gabbro, quartz monzonite, granodiorite porphyry, granodiorite, quartz diorite, adamellite, tonalite, granite and hornblende andesite are high. In contrast, the magnetic susceptibilities of quartz diorite porphyry, pyroxene diorite porphyrite, diorite porphyrite, andesitic porphyrite and pyroxene andesite are low, and their resulting magnetic anomalies are difficult to recognize where they are the spatially superimposed by andesites and granites (Table 1).

Rocks that are characteristically magnetite bearing, such as magnetite mineralized marble and magnetite mineralized skarn, have high magnetic susceptibilities. The magnetic susceptibilities of sedimentary rocks are generally very lowl or zero, which are good candidates for studying deep magmatic activity of the lithosphere using magnetic data (Table 1).

Aeromagnetic data in South China

Data collection and processing

The aeromagnetic data used in this study are presented at a scale of 1:1,000,000 [grid cell size of 0.05° (~5 km)] (Fig. 2a) and were generated by the China Geological Survey in 2009. The longitude range of the data is from 102°E

Table 1 Magnetic susceptibility statistics of the rocks in South China (Geological Survey of Jiangsu Province, China 2015)

Serial number	Rock names	Samples number	Magnetic susceptibility/K × 10^{-5} SI	
			Value scope	Average value
1	Basalt	3	2500–153,230	8040
2	Andesitic basalt	4	140–1130	750
3	Andesitic breccia	45	30–2850	630
4	Andesite	46	0–1860	500
5	Trachyte	80	0–1040	160
6	Tuff	90	0–1760	210
7	Gabbro	369	150–63,430	12,560
8	Quartz diorite	100	0–3640	1510
9	Quartz diorite porphyry	376	40–11,620	1630
10	Quartz monzonite	476	280–11,930	2640
11	Granodiorite	817	20–8040	1510
12	Granite	311	450–2890	1380
13	Porphyritic quartz monzonite	335	20–14,190	1510
14	Quartz diorite porphyry	45	20–9875	700
15	Pyroxene diorite porphyrite	399	0–137,820	440
16	Diorite porphyrite	604	0–37,550	400
17	Pyroxene andesitic porphyrite	51	0–4870	150
18	Andesitic porphyrite	119	15–4750	580
19	Hornblende andesite	245	0–12,690	1290
20	Magnetite mineralized marble	11	13,440–89,550	31,150
21	Magnetite mineralized skarn	448	30–286,370	9420

to 121°E and the altitude range is from 16.1°N to 37°N. A series of processing procedures were adopted to suppress noises, extract and strengthen useful information and enhance the geological interpretation ability of the magnetic anomalies (Zhu and Lu 2016). In this study, we use reduction to pole, low-frequency filtering, derivative calculation in the vertical direction, boundary enhancement and analytical signal amplitude analysis during the processing of aeromagnetic data (Ranganai et al. 2016; Kadasi 2015; Zhu and Lu 2016). The principal processing procedures are described in detail as follows.

The first step is the reduction to pole mainly for removing the skewness of the magnetic anomalies. The basic parameters of magnetic field were chosen according to the international reference geomagnetic field (Thébault et al. 2010; Zhu and Lu 2016). The declination (D) and the inclination (I) of the normal magnetic field in the study area were −2.46353° and 40.8977°, respectively.

The second step is low-frequency filtering. Only low-frequency signals from 0 Hz to the cutoff frequency are used by blocking or weakening higher-frequency signals. The magnetic anomalies caused by the high-frequency magnetic interferences near the surface can be attenuated or depressed through the low-frequency filtering procedure (Zhu and Lu 2016). The shapes of magnetic anomalies will gradually become simple with this procedure and the anomalies with low-frequency bandwidth caused by the large magnetic bodies can be highlighted. This procedure is beneficial for understanding the magnetic characteristics of deep geological bodies and has also helped to deduce the depths and spatial distributions of geological bodies (Zhu and Lu 2016). It is useful for deducing the basement structures and for inferring concealed rock bodies. In this study, we conducted the low-frequency filtering procedure with three different cutoff wavelengths (4 m, 10 m and 30 m) based on the magnetic ΔT anomaly with reduction to pole.

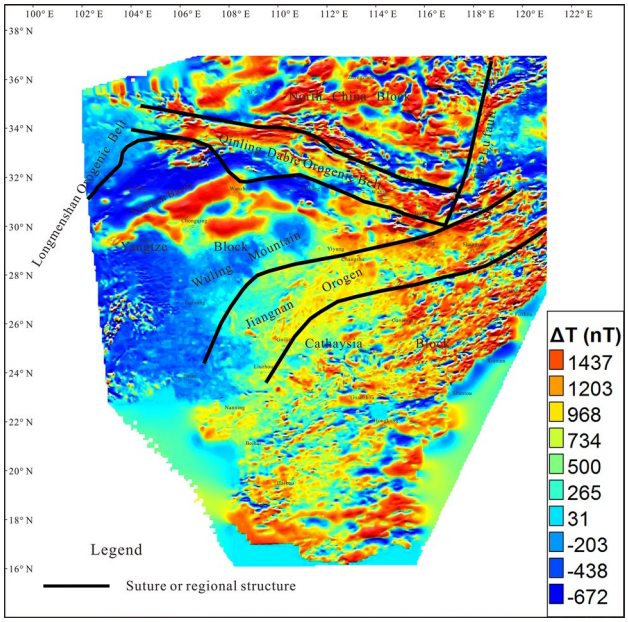

Fig. 2 Observed aeromagnetic anomaly (Δ*T*) distribution of South China, where nT is the unit of magnetic data

The third step is to calculate the derivative of the magnetic Δ*T* anomaly to eliminate the background anomalies of the normal fields, depress the effects of the regional field, separate the superposed anomalies and distinguish the anomalies caused by adjacent magnetic bodies (Zhu and Lu 2016). The procedure can decrease the background magnetic interferences superposed in local magnetic fields and those magnetic interferences from surrounding rocks with small magnetic susceptibilities (Wang et al. 2010b; Kadasi 2015; Eppelbaum 2015; Zhu and Lu 2016). The zero line of the second-order derivative in vertical direction based on the magnetic Δ*T* anomaly with reduction to pole can be used to trace magnetic anomalies of buried bodies and deduce their locations and scopes. In this paper, we calculated the first- and second-order derivatives in the vertical direction based on the magnetic Δ*T* anomaly with reduction to pole and low-frequency filtering with different cutoff wavelengths (4 m, 10 m and 30 m) of the magnetic Δ*T* anomaly with reduction to pole.

The fourth step is boundary enhancement calculation to enhance the fracture structure information, depress the non-structural information and identify the positions of fractures or the boundaries of magnetic bodies. It can overcome the influences of both shallow and deep sources of interference and provide accurate information on fracture location if combined with the low-frequency filtering procedure during data processing (Wang et al. 2009, 2014; Zhu and Lu 2016). In this paper, we use the tilt derivative (Miller and Singh 1994) for boundary enhancement calculation. The complex analysis signal for a 2D structure is (Miller and Singh 1994; Verduzco et al. 2004)

$$A(x,z) = |A|\exp(j\theta) = \sqrt{\left(\frac{\partial T}{\partial x}\right)^2 + \left(\frac{\partial T}{\partial z}\right)^2} \times \exp\left(j\tan^{-1}\right)\left(\frac{\partial T}{\partial z}\Big/\frac{\partial T}{\partial x}\right), \quad (1)$$

where T is the magnitude of the total magnetic intensity (TMI), $\theta = \tan^{-1}\left(\frac{\partial T}{\partial z}\Big/\frac{\partial T}{\partial x}\right)$ is the local phase and $|A| = \sqrt{\left(\frac{\partial T}{\partial x}\right)^2 + \left(\frac{\partial T}{\partial z}\right)^2}$ is the analytic signal amplitude (AS).

The tilt derivative is the absolute value of the horizontal derivative in the denominator, which serves as an automatic gain control filter and tends to equalize the amplitude output of TMI anomalies across a grid (Verduzco et al. 2004). The tilt derivative is

$$\mathrm{TDR} = \tan^{-1}\left[\frac{\mathrm{VDR}}{\mathrm{THDR}}\right], \tag{2}$$

where VDR and THDR are the first-order vertical and total horizontal derivatives of the TMI, respectively (Miller and Singh 1994; Verduzco et al. 2004). For a grid, VDR and THDR are (Miller and Singh 1994; Verduzco et al. 2004)

$$\mathrm{VDR} = \frac{\partial T}{\partial z}, \text{ and } \mathrm{THDR} = \sqrt{\left(\frac{\partial T}{\partial x}\right)^2 + \left(\frac{\partial T}{\partial y}\right)^2}, \text{ respectively.} \tag{3}$$

In this paper, we calculated the boundary enhancement based on the magnetic ΔT anomaly with reduction to pole and low-frequency filtering with different cutoff wavelengths (4 m, 10 m and 30 m) of the magnetic ΔT anomaly with reduction to pole.

The last step is the signal amplitude calculation and analysis of the magnetic ΔT anomaly with reduction to pole to deduce the boundaries and center of magnetic bodies (Zhu and Lu 2016). The position of the peak signal amplitude values can be regarded as the boundaries of magnetic bodies in the situation that the sensor is close to the magnetic bodies; otherwise, they will be considered as the center of magnetic anomaly bodies when the sensor is far from the magnetic bodies (Huang and Guan 1998; Wang et al. 2014; Zhu and Lu 2016). In this study, we conducted the processing procedure based on the aeromagnetic ΔT anomaly with reduction to pole and low-frequency filtering of the RTP maps filtered with different cutoff wavelengths (4 m, 10 m and 30 m).

Lateral variation of the aeromagnetic anomalies

The comprehensive structural interpretation presented here is based on magnetic anomaly characteristics of aeromagnetic data reduced to pole integrated with the regional geological information from SCB. These characteristics will be helpful to reveal the regional tectonic framework of the SCB. According to the properties of aeromagnetic anomalies in Fig. 2, it is apparent that magnetic anomalies are weak in the southwestern and northwestern parts of the study area and the anomaly values are around the range of −670 to 31 nT; they are strong in the southeast and the anomaly values are almost in the range of 500–1300 nT; and they are the strongest and generally vary quickly in the north, where the values are probably in the range of 1200–1400 nT. The magnetic anomalies are also strong in the east and their peak values are intensive and distributed widely.

The values of the magnetic anomalies vary quickly in the areas of the Longmenshan orogenic belt, Qinling–Dabie orogen and Tan-Lu fault, where they are easily recognized as mainly positive anomalies in the shapes of irregular strips or beads. The negative anomalies are mainly distributed as massive or narrow strips, which are scattered along those to the east of the Jiangnan orogen (Fig. 2). Either the positive magnetic anomalies or the negative ones vary greatly to the northwest, where their gradients change quickly and their magnitudes are high. In the Longmenshan belt, the positive and negative magnetic anomalies are alternately distributed along an anomaly gradient belt, with the positive anomalies being strong and widely distributed as massive and irregular strips. There are big negative magnetic anomalies in the northwestern part of the Longmenshan belt and there are small negative anomalies in the Sichuan Basin. From the Wuling Mountain to the east, the values of magnetic anomalies are small and their shapes are distributed broadly. The positive magnetic anomalies in the Jiangnan orogen are intensive and their peak values are small. There is a broad belt of positive magnetic anomalies from SW to NE in the eastern part of the Jiangnan orogen and the belt extends to the southwest until it meets the Tan-Lu fault. There are many local big and positive magnetic anomalies distributed in the ENE direction and in the shapes of narrow strips among the belt. In general, there are mainly positive magnetic anomalies, which are scattered in the areas of broadly distributed negative anomalies.

Based on the distributions of magnetic anomalies (Fig. 3), it is obvious that the characteristics of those in the Jiangnan orogen are different in both peak intensities and shapes from those in the Sichuan Basin and the Wuling Mountain.

The values of positive magnetic anomalies in the Jiangnan orogen are small and those anomalies are continuously distributed along a northeasterly trend. The positive anomalies in the Jiangnan orogen are distributed as strips and small masses to the SW–NE, and their peak values are big and concentrated, which indicates that magmatic rocks are distributed widely therein. The other parts in the Jiangnan orogeny are mainly characterized by negative magnetic anomalies, revealing that a unified and widely distributed strong magnetic basement does not exist in its deep region. It can be deduced from the magnetic anomalies characteristics that there are some near parallel SW–NE-trending faults in the SE of the SCB (Fig. 3).

The magnetic anomalies changed gradually from small values to big positive ones along the Qinling–Dabie orogenic belt from west to east. There are several obvious magnetic gradient belts from the northeast of the Longmenshan belt to the Qinling–Dabie orogenic belt. The positive anomalies in the area of the Dabie Mountain Range vary in the orientation from NW to NE. The orientations of these anomalies are similar to those of the present day Dabie Mountain Range.

The distribution of the magnetic anomaly values become gradually monotonous in RTP maps filtered with increasing cutoff wavelengths, indicating the regional distribution of deeply buried rock units in the SCB (Fig. 3). The negative anomaly values in the Sichuan Basin is distributed more

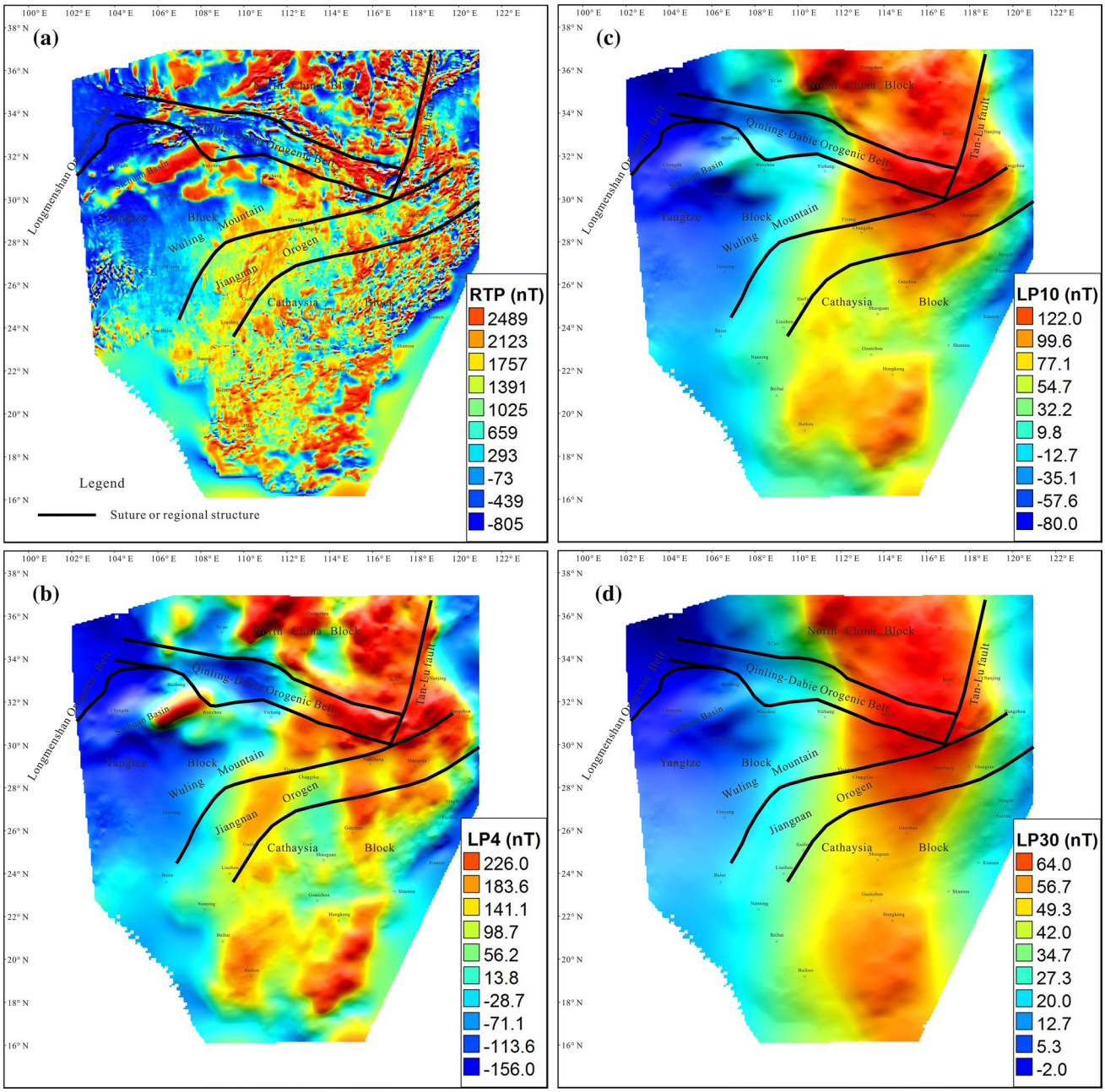

Fig. 3 Aeromagnetic anomaly with reduction to pole (**a**), and low-frequency filtered RTP maps with different wavelengths **b** 4 m, **c** 10 m and **d** 30 m. Note that LP4 indicates the filtered RTP map with a wavelength of 4 m

and more broadly in RTP maps filtered with increasing cutoff wavelengths, revealing that the Sichuan Basin is an independent craton (Fig. 3). It can be seen in Fig. 3d that the magnetic anomaly characteristics are clearly different between the eastern and western sides of the Jiangnan orogen. A belt of broad positive anomalies is present on its eastern side, within which there are widely distributed negative anomalies (Fig. 3). Therefore, the differences in anomaly characteristics between the two different sides of the Jiangnan orogen indicate that there are two separate blocks in South China. The Cathaysia Block, on the east of the Jiangnan orogen, contains numerous faults, which provide magmatic transport pathways for frequent magmatic activities, and these broad magnetic anomalies are present that result from the widely distributed magmatic rocks (Fig. 4). However, the Yangtze Block, on the west of the Jiangnan orogen, stably contains few faults with associated magmatic activities, and there are accordingly few outcrops of igneous rocks therein. The positive anomalies reveal the regional orogenic belts and the Jiangnan orogen, whereas the negative

anomalies are generally concentrated in the Sichuan Basin and the Minshan area on the north of the Longmenshan belt (Fig. 4).

The anomalies in the eastern side of the Jiangnan orogen generally reveal the same basement as that of the Cathaysia Block, thereby indicating the approximate extent of the Cathaysia Block (Fig. 5). There are three distinct belts of anomalies distributed in the vertical direction in the SCB and they change to two belts in the RTP maps filtered with increasing cutoff wavelengths (Fig. 5). The band of anomalies beneath the Jiangnan orogen disappears in the RTP map filtered with a large cutoff wavelength (Fig. 5d), which indicates that the SCB is composed of two main blocks.

Although the basement of the SCB is thought to be composed of two blocks, Fig. 5 reveals that there are some obvious differences between the magnetic anomalies of these blocks in the horizontal direction. The Yangtze Block is composed of a positive anomaly zone in the south and a

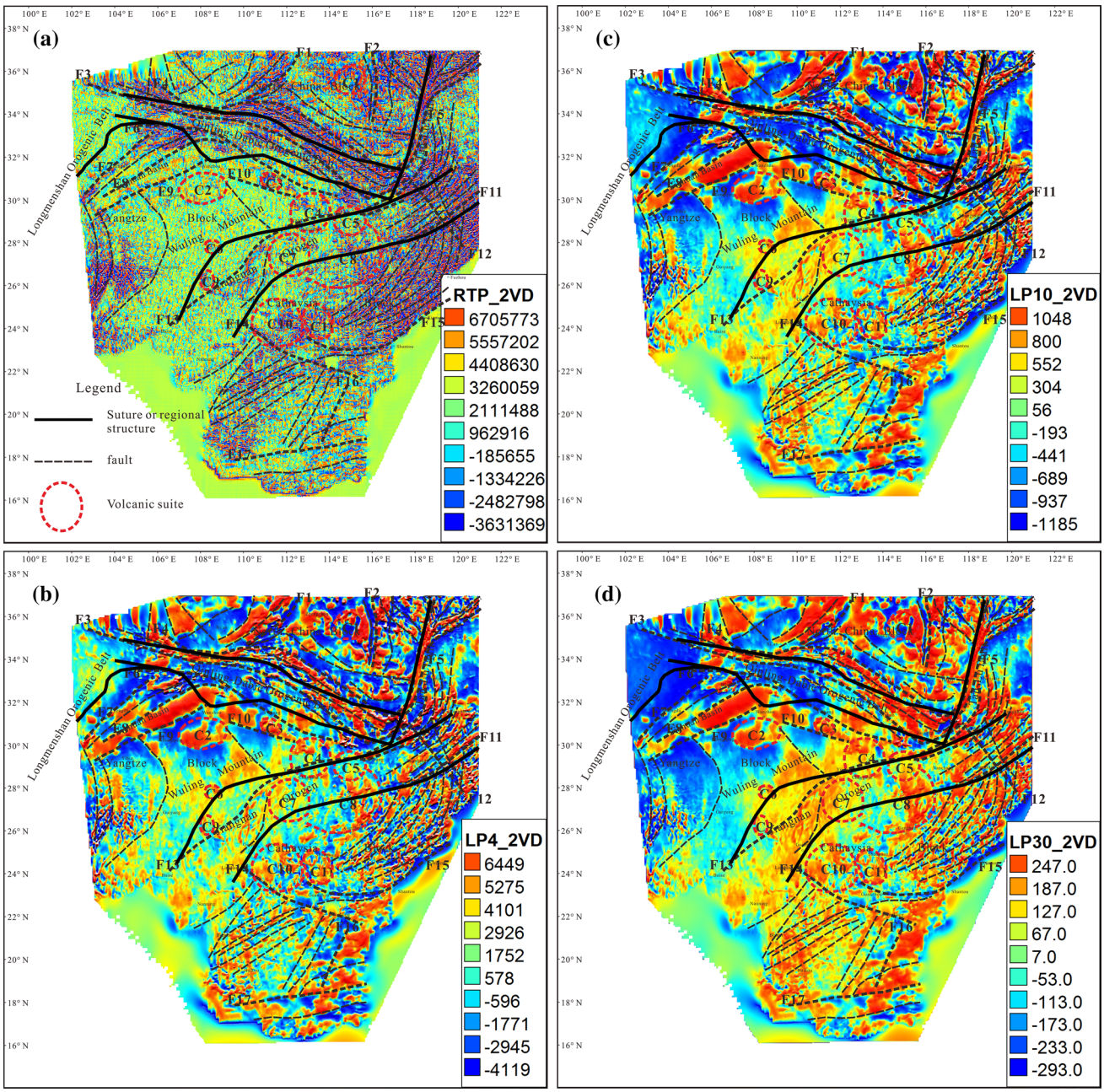

Fig. 4 The second-order derivative in vertical direction of the RTP map (**a**), and the low-frequency filtered RTP maps (**b**–**d**), as shown in Fig. 3. Note that different scales are for maps. For details, see text. Also shown in the figure are sutures (black lines), main fault systems (black dashed lines) and volcanoes (red dashed lines)

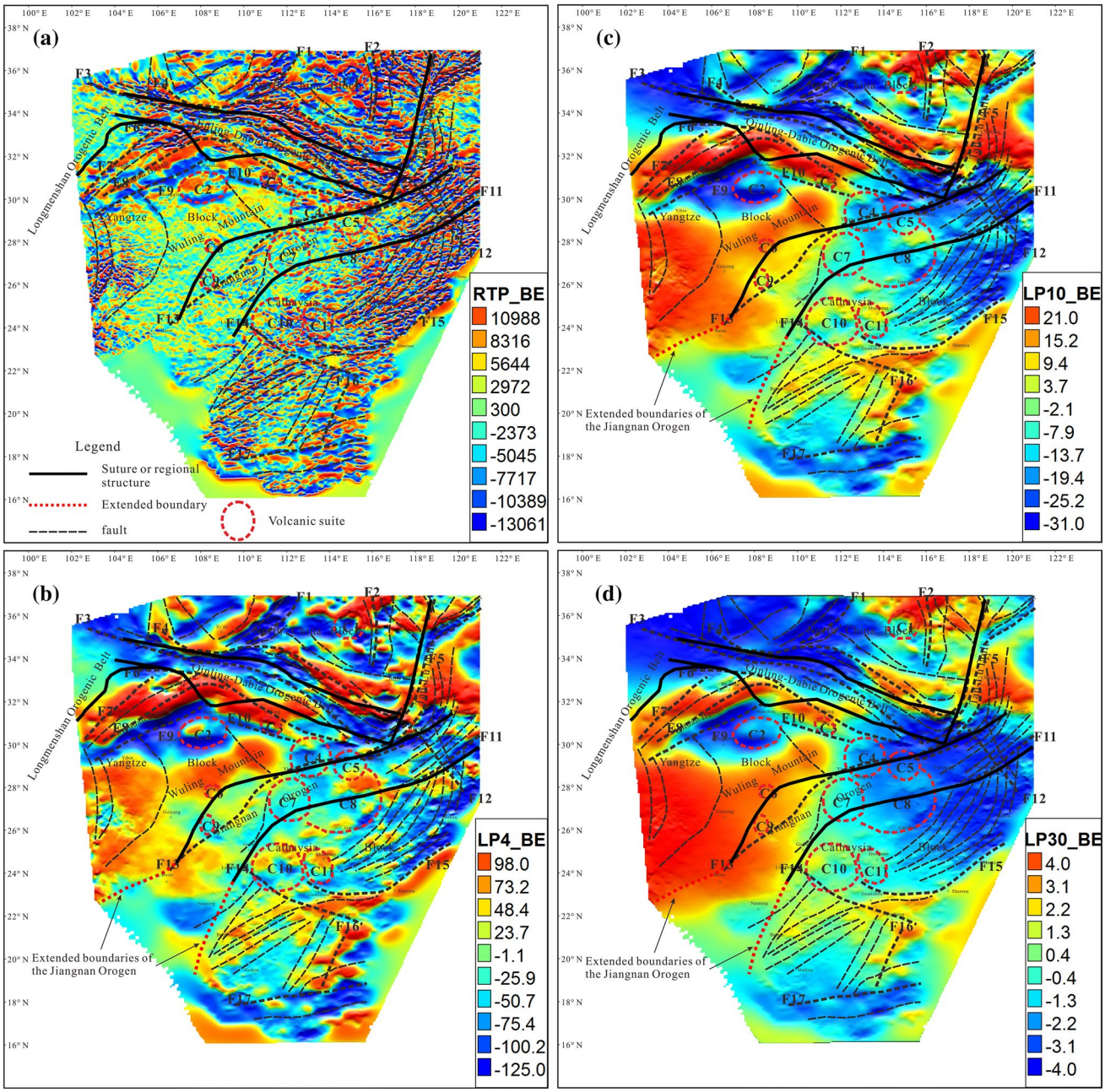

Fig. 5 Boundary enhancement in horizontal direction of the RTP map (**a**), and the low-frequency filtered RTP maps (**b**–**d**), as shown in Fig. 3. Note that different scales are for maps. For details, see text. Also shown in the figure are sutures (black lines), main fault systems (black dashed lines) and volcanoes (red dashed lines)

negative anomaly zone in the north (Fig. 5). The Cathaysia Block is composed of three different anomaly zones (Fig. 5), that is, two negative anomaly zones that are separated by one positive anomaly zone from the south to north. The negative anomaly zone on the north side represents the main part of the Jiangnan orogen (Fig. 5).

The peak values of analytic signal amplitudes are distributed mainly along the structural belts, especially along the Qinling–Dabie orogenic belt and the Longmenshan orogenic belt (Fig. 6). In the east of the Jiangnan orogen, the peak values are concentrated and distributed along a broad belt in the SW–NE direction. These peak values decrease gradually in the RTP maps filtered with increasing cutoff wavelengths and disappear altogether at the RTP map filtered with a 30 m cutoff wavelength (Fig. 6d). This indicates that the Cathaysia Block has a uniform basement and most of the faults in the block do not extend into the deep basement. In the west of the Jiangnan orogen, the analytic signal amplitudes have

more massive forms and are broad with less variation of amplitude gradients. This indicates that the Yangtze Block is composed of a relatively uniform basement, especially for the Sichuan Basin.

Most of volcanic suites are the residual bodies of ancient volcanoes that were destroyed during subsequent geological processes. Their constituents include intrusive rocks, subvolcanic rocks, volcanic rocks in volcanic vents, erupted volcaniclastic rocks and others (Zhu and Lu 2016). In the magnetic anomaly maps, most of the volcanic rocks appear as rings of alternating positive and negative values, as approximate circular shapes or as chain-like shapes distributed along faults (Zhou and Wu 1983; Zhu and Lu 2016). Five different kinds of volcanic suites have been summarized (Zhou and Wu 1983; Zhu and Lu 2016): those that generated magnetic anomalies with almost equal areas and in

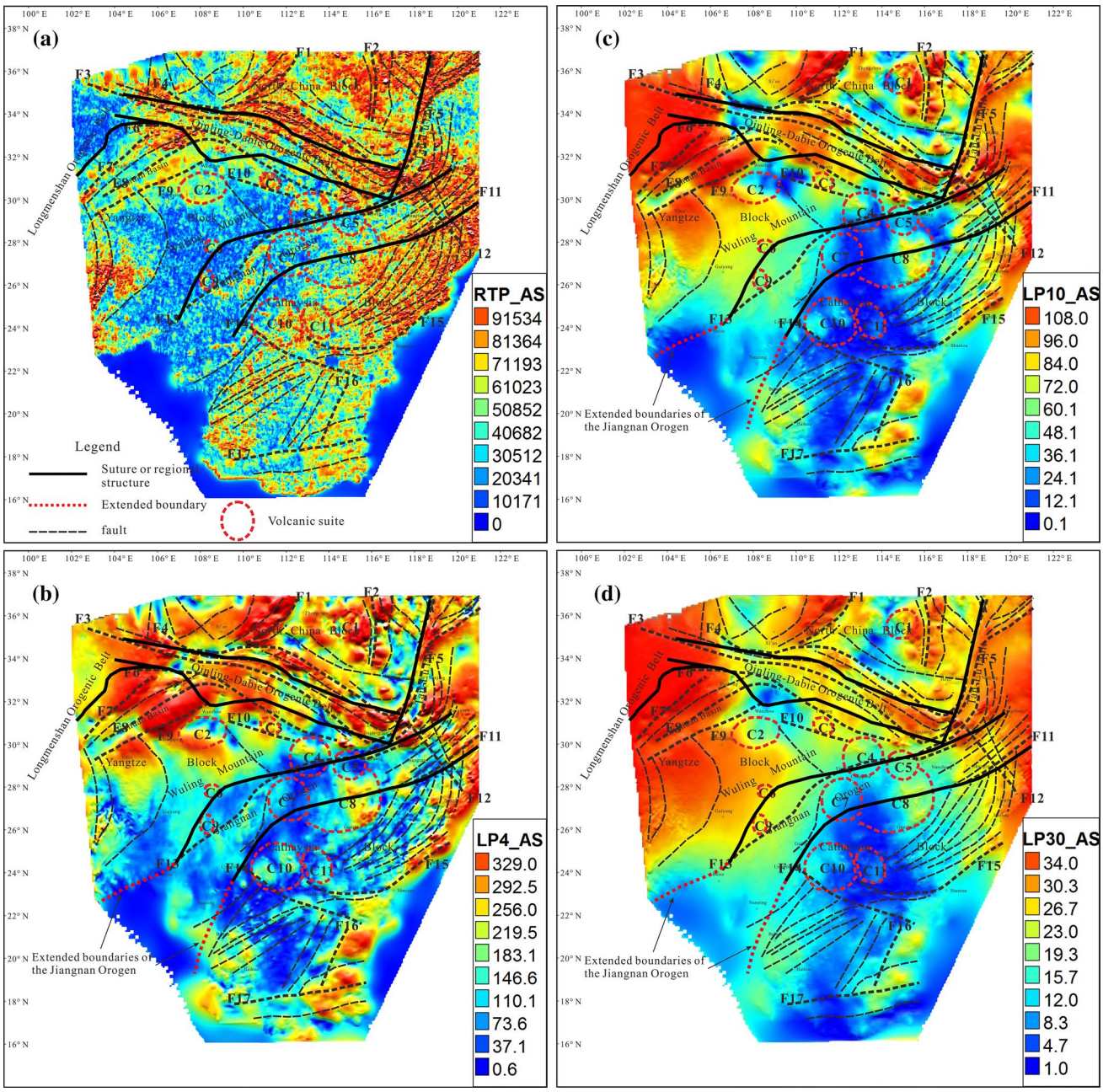

Fig. 6 Analytic signal amplitude analysis of the RTP map (**a**), and the low-frequency filtered RTP maps (**b**–**d**), as shown in Fig. 3. Note that different scales are for maps. For details, see text. Also shown in the figure are sutures (black lines), main fault systems (black dashed lines) and volcanoes (red dashed lines)

single-axial shapes (or similar to single-axial shapes), which were caused by ultrabasic, basic or intermediate rocks in volcanic vents; those showing strong multi-peak or multi-axial radial anomalies, which were formed by the volcanic vents with dominative intermediate-acid erupted volcanic ashes; those consisting of anomalies with sharp gradient changes and disorderly ring banded anomalies with alternating positive and negative values, formed by volcano depressions or volcano domes; those formed from the fissures' eruptions controlled by the basement faults, which showed beaded arrangement and strong magnetic anomalies belts; and those that have a single strong negative anomaly caused by rocks with reverse magnetization in smooth negative magnetic fields. These classifications of volcanic suites provide an effective means for recognizing them in the aeromagnetic data (Zhu and Lu 2016).

In the second-order derivative calculation presentation (Fig. 4), the volcanic suites typically form ring anomalies with alternative positive and negative anomaly values, with peak values situated in the middle of the rings and anomaly values are distributed in the shapes of ring. Most of the volcanic suites are beaded in form and distributed along the N–S trending deep, regional faults, particularly in the south of the Qinling–Dabie orogenic belt. Some volcanic suites near the Jiangnan orogeny are also distributed at the areas of intersecting faults with NE–SW orientations (Fig. 6).

Discussion

In the Mesoproterozoic, the dominant tectonic framework of SCB are composed of some separated terranes, the Yangtze block and the Cathaysia block are separated terranes and both of them are composed of some micro-plates (or micro-continents) (Zhang et al. 2013). In the early and middle Neoproterozoic, during the assembling process of Rodinia supercontinent, the Yangtze and Cathaysia blocks are formed with the assembling of different micro-plates, and then the unified SCB was formed during the collision process (or amalgamation) between the separated Yangtze and Cathaysia blocks along the south Anhui province–east Xuefeng-Miaoling areas in the middle Neoproterozoic (Wang et al. 2003; Shu et al. 2011; Shu 2012; Zhang et al. 2013). The probable collision boundary between the Yangtze and Cathaysia blocks in the Neoproterozoic are shown in solid lines in Fig. 7a–c, which are nearly in the NS direction.

We may extend the possible southwestern boundaries of the Jiangnan orogen (show in red dashed lines in Fig. 5c, d), which are not clear in previous studies of the South China Block (Shu et al. 2011; Shu 2012; Zhang et al. 2013), according to the boundary enhancement in horizontal direction of the RTP maps (Fig. 5b–d). These extension boundaries are more and more clear in the RTP maps filtered with increasing cutoff wavelengths.

In the RTP maps filtered with different cutoff wavelengths (Fig. 7a–c), the ranges of positive magnetic anomalies in the Jiangnan orogeny gradually decrease with the increasing cutoff wavelengths (Fig. 7b, c) and the positive magnetic anomalies disappear in the RTP maps filtered with a cutoff wavelength of 30 m (Fig. 7a), thereby indicating the strong magnetic basement in the Jiangnan orogeny is buried in shallow in the crust. The magnetic anomalies characteristics are completely inconsistent between the shallow (Fig. 7b, c) and deep (Fig. 7a) regions in the Jiangnan orogeny, revealing that there are some inconsistencies between the shallow cover and the deep basement therein. Therefore, there should exist an extension-detachment structure in the Jiangnan orogeny.

It can be seen in Fig. 7a that the micro-plates, which composed the Yangtze block, have nearly homogeneous negative magnetism in the western side and the magnetism increases gradually from west to east. The Cathaysia block is composed by two dominant plates and both of them have positive magnetism. For the two dominant plates, the one at the northeastern side is relatively bigger than that in the southwestern side, and they assembled along the northeastern boundary shown by dashed lines in Fig. 7a–c.

During the breakup process of the Rodinia supercontinent (800–720 Ma), the terranes of the unified South China plate began to separate into two main terranes (or rifting activity) along the northeast direction forming the Nanhua and Sichuan–Yunnan rift basins (Wang et al. 2003; Zhang et al. 2013). Zhang et al. (2013) regard that the dividing boundary between the Meso- and Neoproterozoic Yangtze and Cathaysia blocks is along the original position of the Fuchuan–Jiuling–Yiyang–Sibao line. We can find the rifting boundary, which separated the unified SCB into two continental blocks in the lithosphere, shown by dashed lines in Fig. 7d–f and the two lines are distributed mainly along the NS and NW direction. The arrows in Fig. 7d–f show the probable movement directions of terranes. In the Cathaysia Block, there is a rift between the two micro-plates along the WE direction.

The distributions of magnetic anomaly in Fig. 7d–f show the extended areas of magmatic activity in east South China plate, which causes planar distribution of granites. There are two broad strong magnetism belts separated by a low magnetism belt along the northeast direction in the east SCB. There are some sedimentary strata in the rift basins, which show low magnetism in Fig. 7d. In the meanwhile, from Fig. 7d–f, it can be found that there are some new small plates being generated in the separating surroundings and there are some rift basins formed inside both the Yangtze and Cathaysia blocks (Zhang et al. 2013).

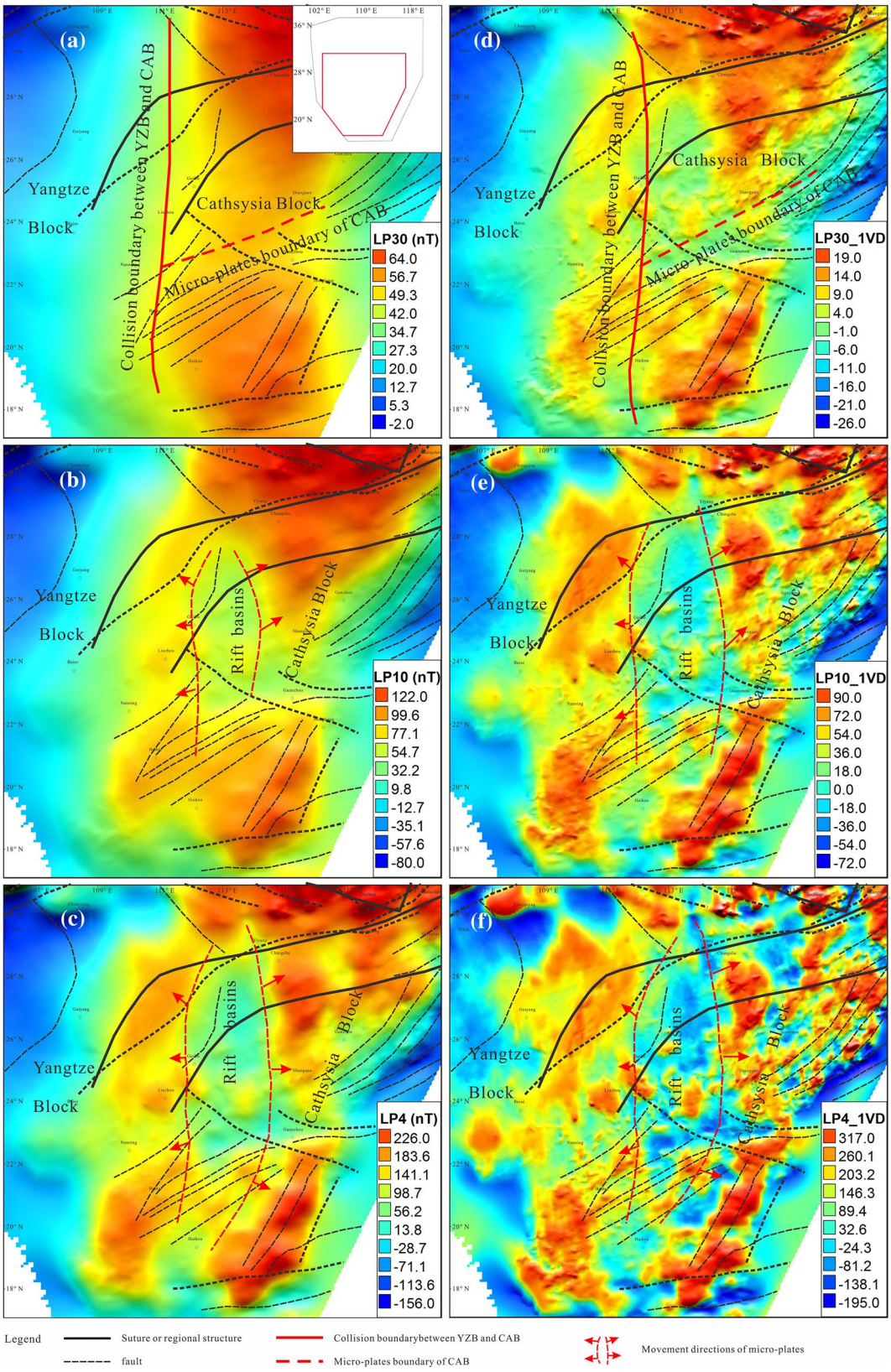
(a)
Yangtze Block
Cathsysia Block
Collision boundary between YZB and CAB
Micro-plates boundary of CAB
LP30 (nT)
64.0
56.7
49.3
42.0
34.7
27.3
20.0
12.7
5.3
-2.0
(d)
LP30_1VD
19.0
14.0
9.0
4.0
-1.0
-6.0
-11.0
-16.0
-21.0
-26.0
(b)
Rift basins
LP10 (nT)
122.0
99.6
77.1
54.7
32.2
9.8
-12.7
-35.1
-57.6
-80.0
(e)
LP10_1VD
90.0
72.0
54.0
36.0
18.0
0.0
-18.0
-36.0
-54.0
-72.0
(c)
LP4 (nT)
226.0
183.6
141.1
98.7
56.2
13.8
-28.7
-71.1
-113.6
-156.0
(f)
LP4_1VD
317.0
260.1
203.2
146.3
89.4
32.6
-24.3
-81.2
-138.1
-195.0
Legend
Suture or regional structure
fault
Collision boundarybetween YZB and CAB
Micro-plates boundary of CAB
Movement directions of micro-plates

◂**Fig. 7** Local RTP maps and local the first-order derivative in vertical direction of the RTP maps. Low-frequency filtered RTP maps with different wavelengths **a** 30 m, **b** 10 m and **c** 4 m; the first-order derivative in vertical direction of the low-frequency filtered RTP maps with different wavelengths **d** 30 m, **e** 10 m and **f** 4 m. The red polygon at the top right corner of **a** shows the local scope of image. Note that different scales are for maps. For details, see text. Also shown in the figure are sutures (black lines), main fault systems (black dashed lines), collision boundary between YZB and CAB (red lines), micro-plates boundary of CAB (red dashed lines) and movement directions of micro-plates (red arrows)

Because the magnetic anomalies in Fig. 7d–f are nearly distributed broadly and homogeneously in the east SCB, these granites lacked the mantle component material, that is, they were not generated from the subduction and collision between different plates, but from the interaction between the Yangtze and Cathaysia blocks. Therefore, an intracontinental tectonic evolution was followed in the Phanerozoic in the South China plate (Zhou and Li 2000; Wan et al. 2007; Shu 2012; Zhang et al. 2013).

The distribution of near surface structures shown in Figs. 4, 5 and 6 are summarized from the interpreted faults and volcanic suites mentioned above. Eleven small volcanic suites (C1 to C11) have been identified and most of them are distributed around the peak values of analytic signal amplitudes (Fig. 6). We have also interpreted 17 regional deep faults (F1 to F17); the strikes and some aeromagnetic anomaly properties of these faults are shown in Table 2.

In this paper, we deduce the structural features of the SCB based on the magnetic characteristics of aeromagnetic data at a certain depth, and the magnetic characteristics are the comprehensive magnetism results of different depths in the lithosphere, which are superimposed on a plane. Therefore, in this paper, the structural features based on the aeromagnetic data maybe not exactly consistent with the structure information deduced from surface geology.

Conclusion

In this paper, we reach several conclusions based on the processing and interpretation of the aeromagnetic data integrated with the regional geological and structural information of the South China Block. We describe the magnetic anomaly characteristics of the South China Block, as well as the Qinling–Dabie orogeny and Longmenshan belt. We have extended the possible southwestern boundaries of the Jiangnan orogen which are not clear in previous studies of South China. We have ascertained some faults and volcanic suites, which reveal the regional tectonic framework of the South China Block. We reveal the magnetic anomaly boundary between the Yangtze and Cathaysia blocks in the Neoproterozoic in the South China Block. We provide the aeromagnetic evidences for an intracontinental interaction between the Yangtze and Cathaysia blocks, not a subduction and collision between different plates, which followed in the Phanerozoic in the South China Block. This study provides some basic information on the geology, structural characteristics and geodynamics in the South China Block.

Table 2 Attributes of regional deep faults deduced from the aeromagnetic data in South China

Serial number	Fault name	Trend of fault	Characteristics of aeromagnetic field
1	F1	NE-SN	Gradient variation belt, discontinuity and dislocation belt
2	F2	SN	Gradient variation belt, discontinuity and dislocation belt
3	F3	NW-NE	Bead-like anomalies belt, discontinuity and dislocation belt
4	F4	NW-NE	Bead-like anomalies belt, discontinuity and dislocation belt
5	F5	SN-NE	Gradient variation belt, discontinuity and dislocation belt
6	F6	EW-NW	Bead-like anomalies belt, discontinuity and dislocation belt
7	F7	NE	Bead-like anomalies belt, discontinuity and dislocation belt
8	F8	NE	Gradient variation belt, discontinuity and dislocation belt
9	F9	NE	Gradient variation belt, discontinuity and dislocation belt
10	F10	NW	Gradient variation belt
11	F11	NE	Bead-like anomalies belt, discontinuity and dislocation belt
12	F12	NW	Bead-like anomalies belt, discontinuity and dislocation belt
13	F13	NE-EW-NE	Bead-like anomalies belt, discontinuity and dislocation belt
14	F14	NW	Bead-like anomalies belt, discontinuity and dislocation belt
15	F15	NW-EW-NE	Bead-like anomalies belt, discontinuity and dislocation belt
16	F16	NE	Gradient variation belt, discontinuity and dislocation belt
17	F17	EW-NE	Bead-like anomalies belt, discontinuity and dislocation belt

Acknowledgements This work was jointly funded by the National Science Foundation of China (Nos. 41404070 and 41374101) and China Geological Survey (Nos. DD20190448 and DD201609-05).

References

Charvet J (2013) The Neoproterozoic-Early Paleozoic tectonic evolution of the South China Block: an overview. J Asian Earth Sci 74:198–209

Charvet J, Shu L, Shi Y, Guo L, Faure M (1996) The building of south China: collision of Yangtze and Cathaysia blocks, problems and tentative answers. J SE Asian Earth Sci 13:223–235

Charvet J, Shu L, Faure M, Choulet F, Wang B, Lu H, Breton NL (2010) Structural development of the Lower Paleozoic belt of South China: genesis of an intracontinental orogeny. J Asian Earth Sci 39(4):309–330

Chen J, Jahn BM (1998) Crustal evolution of Southeastern China: Nd and Sr isotopic evidence. Tectonophysics 284:101–133

Chen J, Foland K, Xing F, Xu X, Zhou T (1991) Magnatism along the southeast margin of the Yangtze block: precambrian collision of the Yangtze and Cathaysia blocks of China. Geology 19(8):815–818

Chen X, Rong J, Rowley D, Zhang J, Zhang Y, Zhan R (1995) Is the early Paleozoic Banxi ocean in South China Necessary? Geol Rev 41:389–400 **(in Chinese with English abstract)**

Chu Y, Faure M, Lin W, Wang Q (2012a) Early Mesozoic tectonics of the South China Block: insights from the Xuefengshan intracontinental orogeny. J Asian Earth Sci 61:199–220

Chu Y, Faure M, Lin W, Wang Q, Ji W (2012b) Tectonics of the Middle Triassic intracontinental Xuefengshan Belt, South China: new insights from structural and chronological constraints on the basal decollement zone. Int J Earth Sci 101:2125–2150

Chu Y, Lin W, Faure M, Wang Q, Ji W (2012c) Phanerozoic tectonothermal events of the Xuefengshan Belt, central South China: implications from U-Pb age and Lu-Hf determinations of granites. Lithos 150:243–255

Deng Y, Zhang Z, Badal J, Fan W (2014) 3-D density structure under South China constrained by seismic velocity and gravity data. Tectonophysics 627:159–170

Ding D, Guo T, Hu M, Liu Y (2007) Basement decoupling structure in Jiangnan Xuefeng-Series 1 of the southern structure studies. Pet Geol Exp 29(2):120–128 **(in Chinese with English abstract)**

Eppelbaum LV (2015) Quantitative interpretation of magnetic anomalies from bodies approximated by thick bed models in complex environments. Environ Earth Sci 74:5971–5988

Faure M, Lin W, Chu Y, Lepvrier C (2016) Triassic tectonics of the southern margin of the South China Block. CR Geosci 348(1):5–14

Geological Survey of Jiangsu province, China (2015) Report of the 3D geological survey on the key delta areas of the Yangtze River, 23–45

Guo L, Yu J, Shi Y (1963) Discussion on some problems of tectonics of the Caledonian geosyncline areas in South China. J Nanjing Univ 2:1–17 **(in Chinese)**

Guo L, Lu H, Shi Y, Ma R, Sun Y, Shu L, Jia D, Zhang Q (1996) On the Meso-neoproterozoic Jiangnan island arc: its kinematic and dynamics. Geological Journal of Universities 2(1):1–13 **(in Chinese with English abstract)**

He C, Dong S, Santosh M, Chen X (2013) Seismic Evidence for a Geosuture between the Yangtze and Cathaysia Blocks. South China. Sci Rep 3:2200

Hu L, Cawood AP, Du Y, Yang J, Jiao L (2015) Late Paleozoic to Early Mesozoic provenance record of Paleo-Pacific subduction beneath South China. Tectonics 34(5):986–1008

Huang L, Guan Z (1998) The determination of magnetic causative boundaries using total gradient modules of magnetic anomalies. Journal of East China Geological Institute 21(2):143–150 **(in Chinese with English abstract)**

Kadasi AL (2015) Interpretation of aeromagnetic data in terms of surface and subsurface geologic structures, southwestern Yemen. Arab J Geosci 8(2):1163–1179

Li Z, Li X (2007) Formation of the 1300-km-wide intracontinental orogen and postorogenic magmatic province in Mesozoic South China: a flat-slab subduction model. Geology 35:179–182

Li X, Li Z, Liu Y, Yuan C, Wei G, Qi C (2007) U-Pb zircon, geochemical and Sr-Nd-Hf isotopic constrains on age and origin of Jurassic I- and A-type granites from central Guangdong, SE China: a major igneous event in response to foundering of a subducted flat-slab? Lithos 96:186–204

Li C, Chen S, Zhang P, Yang H, Chen L (2011) Palaeozoic-Mesozoic sedimentary evolution characteristics of the Xuefeng Mountain intracontinental orogenic belt. Geol China 38(1):43–51 **(in Chinese with English abstract)**

Li Y, Gao M, Qu Q (2014) Crustal thickness map of the Chinese mainland from teleseismic receiver functions. Tectonophysics 611:51–60

Liu Y, He Z, Zhang B, Dong W, Li D (2006) Integrated geophysical technique for identification of igneous rocks. Prog Explor Geophys 29(2):115–118 **(in Chinese with English abstract)**

Miller HG, Singh V (1994) Potential field tilt—a new concept for location of potential filed sources. J Appl Geophys 32:213–217

Peng S, Kusky T, Jiang X, Wang L, Wang J, Deng H (2012) Geology, geochemistry and geochronology of the miaowan ophiolite. Yangtze craton: implications for south china's amalgamation history with the rodinian supercontinent. Gondwana Res 21(2–3):577–594

Qiu Y, Zhang Y, Ma W (1998) Tectonics and geological evolution of Xuefeng intra-continental orogene, South China. Geol J China Univ 4(4):433–444 **(in Chinese with English abstract)**

Ranganai RT, Whaler KA, Ebinger CJ (2016) Aeromagnetic interpretation in the south-central Zimbabwe Craton: (reappraisal of) crustal structure and tectonic implications. Int J Earth Sci 105(8):2175–2201

Ren J (2015) International geological map of Asia (1:5,000,000). Geological Publishing House, Beijing

Shu L (2006) Pre-devonian tectonic evolution of South China: from Cathaysia Block to Caledonian folded belt. Geol J China Univ 12(4):418–431 **(in Chinese with English abstract)**

Shu L (2012) An analysis of principal features of tectonic evolution in South China Block. Geol Bull China 31(7):1035–1053 **(in Chinese with English abstract)**

Shu L, Faure M, Yu J, Jahn BM (2011) Geochronological and geochemical features of the Cathaysia block (South China): new evidence for the Neoproterozoic breakup of Rodinia. Precambr Res 187(3–4):263–276

Shu L, Wang B, Cawood AP, Santosh M, Xu Z (2015) Early paleozoic and early mesozoic intraplate tectonic and magmatic events in the Cathaysia block, South China. Tectonics 34(8):1600–1621

Tang S, Yan D, Wang C, Zhang W (2011) Deformational process from thick-skinned to thin-skinned thrust in Xuefeng Mountain, South China: evidence from Sangzhi-Anhua tectonic section. Geoscience 25(1):22–30 **(in Chinese with English abstract)**

Thébault E, Purucker M, Whaler KA, Langlais B, Sabaka TJ (2010) The magnetic field of the earth's lithosphere. Space Sci Rev 155:95–127

Verduzco B, Fairhead JD, Green CM, MacKenzie C (2004) New insights into magnetic derivatives for structural mapping. Lead Edge 23(2):116–119

Wan Y, Liu D, Xu M, Zhuang J, Song B, Shi Y, Du L (2007) SHRIMP U-Pb zircon geochronology and geochemistry of metavolcanic and metasedimentary rocks in Northwestern Fujian, Cathaysia block, China: tectonic implications and the need to redefine lithostratigraphic units. Gondwana Res 12:166–183

Wang J, Li Z (2003) History of Neoproterozoic rift basins in South China: implications for Rodinia breakup. Precambr Res 122:141–158

Wang Y, Fan W, Guo F, Pen T, Li C (2003) Geochemistry of Mesozoic mafic rocks adjacent to Chenzhou-Linwu fault, South China: implications for the lithospheric boundary between the Yangze and Cathaysia Block. International Geology Review 45:263–286

Wang X, Zhou J, Griffin WL, Wang R, Qiu J, O'reilly SY, Xu X, Liu X, Zhang G (2007) Detrital zircon geochronology of Precambrian basement sequences in the Jiangnan origin: dating the assembly of the Yangtze and Cathaysia blocks. Precambr Res 159:117–131

Wang W, Pan Y, Qiu Z (2009) A new edge recognition technology based on the normalized vertical derivative of the total horizontal derivative for potential field data. Appl Geophys 6(3):226–233

Wang Y, Zhang F, Fan W, Zhang G, Chen S, Cawood AP, Zhang A (2010a) Tectonic setting of the South China Block in the early Paleozoic: resolving intracontinental and ocean closure models from detrital zircon U-Pb geochronology. Tectonics 29(6):1–16

Wang W, Zhang G, Liang J (2010b) Spatial variation law of vertical derivative zero points for potential field data. Appl Geophys 7(3):197–209

Wang W, Wang Y, Li J, Liu J, Zhao B, Zhou X (2014) Study on the faults structure and granite body distribution in Pangshan area of Yudu-Ganxian ore district using gravity and magnetic data. Geophys Geochem Explor 38(4):825–834 **(in Chinese with English abstract)**

Xiong S, Liu H, Wang Y, Yin Z, Teng J, Hu H (2002) A study on velocity distribution in upper crust and tectonics of basement and cover in South China. Chin J Geophys 45(6):784–794 **(in Chinese with English abstract)**

Yu J, O'Reilly SY, Wang L, Griffinm WL, Zhou M, Zhang M, Shu L (2010) Components and episodic growth of Precambrian crust in the Cathaysia block, South China: evidence from U-Pb ages and Hf isotopes of zircons in Neoproterozoic sediments. Precambr Res 181(1):97–114

Yuan X, Hua J (2011) 3D Lithospheric structure of South China. Geology China 38:1–19 **(in Chinese with English abstract)**

Zhang S, Zheng Y, Wu Y, Zhao Z, Gao S, Wu F (2006) Zircon isotope evidence for big or equal 3.5 Ga continental crust in the Yangtze craton of China. Precambr Res 146(1):16–34

Zhang G, Guo A, Wang Y, Li S, Dong Y, Liu S, He D, Cheng S, Lu R, Yao A (2013) Tectonics of South China Continent and its implications. Sci China Earth Sci 56(11):1804–1828 **(in Chinese with English abstract)**

Zhao B, Zhang Z, Bai Z, Badal J, Zhang Z (2013) Shear velocity and Vp/Vs ratio structure of the crust beneath the southern margin of South China continent. J Asian Earth Sci 62:167–179

Zheng Y, Zhang S (2007) Formation and evolution of the Precambrian continental crust in South China. Chin Sci Bull 52(1):1–12 **(in Chinese)**

Zhou X, Li W (2000) Origin of Late Mesozoic igneous rocks in Southeastern China: implications for lithosphere subduction and underplating of mafic magmas. Tectonophysics 326:269–287

Zhou J, Wu J (1983) Magnetic anomaly and continental volcanic mechanism. Geology and Exploration 1:49–56 **(in Chinese)**

Zhu X, Lu M (2016) Regional metallogenic structure based on aeromagnetic data in northern Chile. Appl Geophys 13(4):721–735